

## Article

# Physical Analysis and Mathematical Modeling of the Hydrogen Storage Process in the $MmNi_{4.2}Mn_{0.8}$ Compound

Sihem Belkhiria <sup>1,\*</sup>, Abdulrahman Alsawi <sup>2,\*</sup>, Chaker Briki <sup>1</sup>, Saleh M. Altarifi <sup>2,\*</sup>,  
Mohamed Houcine Dhaou <sup>1,2</sup> and Abdelmajid Jemni <sup>1</sup>

<sup>1</sup> Laboratory of Thermal and Energy Systems Studies, University of Monastir, LR99ES31, Monastir 5019, Tunisia

<sup>2</sup> Department of Physics, College of Science, Qassim University, Buraidah 51452, Saudi Arabia

\* Correspondence: sihem\_belkhiria@yahoo.fr (S.B.); ansaoy@qu.edu.sa (A.A.); striefy@qu.edu.sa (S.M.A.);  
Tel.: +216-99067487 (S.B.)

**Abstract:** The results of an experimental and mathematical study into the  $MmNi_{4.2}Mn_{0.8}$  compound's hydrogen storage properties are presented in the present research. Plotting and discussion of the experimental isotherms (P-C-T) for different starting temperatures (288 K, 298 K, 308 K, and 318 K) were carried out first. Then, the enthalpy and entropy of formation ( $\Delta H_0$ ,  $\Delta S_0$ ) were deduced from the plot of van't Hoff. Following that, the P-C-T were contrasted with a mathematical model developed via statistical physics modeling. The steric and energetic parameters, such as the number of the receiving sites ( $n_1$ ,  $n_2$ ), their densities ( $N_{m1}$ ,  $N_{m2}$ ), and the energy parameters ( $P_1$ ,  $P_2$ ) of the system, were calculated thanks to the excellent agreement between the numerical and experimental results. Therefore, plotting and discussing these parameters in relation to temperature preceded their application in determining the amount of hydrogen in each type of site per unit of metal ( $[H/M]_1$ ,  $[H/M]_2$ ) as well as for the entire system  $[H/M]$  versus temperature and pressure besides the absorption energies associated with each kind of site ( $\Delta E^1$ ,  $\Delta E^2$ ) and the thermodynamic functions (free energy, Gibbs energy, and entropy) that control the absorption reaction.

**Keywords:** hydrogen storage; storage (materials); isotherms; temperature; pressure



**Citation:** Belkhiria, S.; Alsawi, A.; Briki, C.; Altarifi, S.M.; Dhaou, M.H.; Jemni, A. Physical Analysis and Mathematical Modeling of the Hydrogen Storage Process in the  $MmNi_{4.2}Mn_{0.8}$  Compound. *Materials* **2024**, *17*, 2237. <https://doi.org/10.3390/ma17102237>

Academic Editor: Jacques Huot

Received: 20 March 2024

Revised: 15 April 2024

Accepted: 21 April 2024

Published: 9 May 2024



**Copyright:** © 2024 by the authors. Licensee MDPI, Basel, Switzerland. This article is an open access article distributed under the terms and conditions of the Creative Commons Attribution (CC BY) license (<https://creativecommons.org/licenses/by/4.0/>).

## 1. Introduction

The use of natural resources is essential to the advancement of both human society and the global economics. According to economists, it is imperative that energy consumption continues to rise for the purpose of advancing economic, cultural, and social development [1]. For example, to achieve a high level of development, the energy consumption per person must be approximately 33% higher than current global consumption [2]. However, the energy tactics used have a significant impact on inequalities in human development [3]. Currently, petroleum-based fuels such as coal, oil, and gas from natural sources provide approximately 95% of the energy required by the world. According to estimates, fossil fuel usage reached 3.3 terawatts (TW) in 2020, up 32% from the year 2000 [4].

Thus, even though fossil fuels still account for the majority of primary energy consumption today, countries all over the world have made the strategic decision to support the consumer revolution and the energy transformation in addition to developing a sustainable, solid, and environmentally friendly energy system [5–8].

Hydrogen is a promising alternative to existing power storage techniques that will be used in constructing our future energy system, including flywheels, power sources, air-compressed pumped water, capacitors that store energy, and others [9]. Thus, hydrogen is a feasible green energy vector due to its clean combustion characteristics, suitability for fuel cell vehicles, and potential energy, which is two-to-three times more performant than gasoline [10]. Nevertheless, before the hydrogen sector can see astronomical growth, a number of challenges must be overcome, just like with most renewable energy sources.

These challenges usually relate to its expensive production, complicated storage, and large-scale use [11]. Therefore, storage is a crucial step toward hydrogen energy carriers [12]. Intrinsically, for commercial and practical uses, hydrogen storage systems must combine energy efficiency, security, and affordable storage costs [13]. One of the most promising storage technologies is the metal hydride form. Metal hydrides offer an appealing combination of high energy densities, safety, and numerous potential uses on both a small and large scale as well as the short and long term [14–19].

AB<sub>5</sub> compounds stand out among the large family of hydrides as highly intriguing metal hydride candidates with very interesting hydrogen storing features since they have a significant storage capacity and safe operating conditions defined by moderate pressure and ambient temperature [20–22]. In reality, a hydrogen storage material needs to have a large hydrogen storage capacity, simple reversibility of the reactions leading to its formation and decomposition, and a low overall hydride cost (raw materials, manufacturing, and processing) for the application in question. It is also necessary to guarantee the long-term presence of natural materials (i.e., metallic resources) [23]. The hydride system (including its protection) should have the lowest possible cost per unit of hydrogen that can be stored reversibly. Other factors to consider include a storage vessel's moderate cost, the cost of auxiliary equipment, the cost of fabrication and installation, and the cost of purchased energy that is not derived from waste or ambient air per storage cycle [24]. On top of that, AB<sub>5</sub>-based compounds continued to receive attention from researchers who are primarily interested in reaction kinetics, cycle stability, and material cost reduction [25–37].

For instance, the expensive lanthanum in LaNi<sub>5</sub> can be substituted with less expensive rare earth elements like Ce [38,39] or a less expensive rare earth alloy made of Ce, Pr, Nd, and La known as mischmetal (Mm), which has been the subject of numerous investigations [40,41]. The compositional modifications have resulted in a 30% reduction in raw material prices when compared to the LaNi<sub>5</sub> alloy [42]. Thus, the MmNi<sub>5</sub> compound has demonstrated intriguing hydrogen storage characteristics, such as straightforward activation [42], elevated stability in the electrode potential [40], and a significant hydrogen storage capacity at room temperature, reaching 1.5% Wt [43]. However, the MmNi<sub>5</sub> compound has an equilibrium pressure of up to 30 bar [44]. This is a significantly higher value than, for instance, the equilibrium pressure of LaNi<sub>5</sub>, which is limited to 2 bar [45]. Given that battery cells clearly operate at atmospheric pressures [46], this suggests a challenging engineering design for gas hydrogen storage, which was totally unworkable in MmNi<sub>5</sub> to be utilized as the anode in a Ni-MH battery cell. In addition, despite the fact that MmNi<sub>5</sub> is highly desirable for stationary applications, there are certain inherent limitations that make it impractical to use. One such limitation is the disproportion that occurs during subsequent hydrogen cycles, which is a serious problem since it reduces the hydrogen storage capacity during cycling [47].

Thus, in order to improve the hydrogen storage properties of the compound MmNi<sub>5</sub>, doping on the Mm and Ni sites is a promising strategy adopted by several researchers [48]. To accomplish this, a variety of metals have been employed, either separately or in combination like Al, Fe, Mn, etc. [45,49–54]. These studies showed that adding a particular dopant element allows for the improvement of the stability of hydrides, the prevention of decomposition, improving the properties of storing hydrogen, and the optimization of the thermodynamic characteristics of the MmNi<sub>5</sub> hydride. For these reasons, we decided to consider a manganese-doped compound in the present investigation. Doping a compound like MmNi<sub>5</sub> with additional manganese is a common strategy for hydrogen storage [55]. Compared to other doping elements, these compounds exhibit fast activation behavior, good corrosion resistance, moderate stability, a noticeable reaction enthalpy, and high catalytic activity [42,56–58]. Manganese hydrides are promising compounds that can store hydrogen reversibly in ambient conditions, according to even recent research [59]. In many energy storage applications such as transport and portable devices, its gravimetric and volumetric storage capacity allows it to compete with batteries while significantly reducing the supporting infrastructure's complexity and cost [60]. The battery's affordability, longevity,

safety, dependability, sustainability, usability, and power or energy makes it a promising material for electric vehicle storage technologies [61]. Manganese doping is a commonly employed technique in metal hydrides to enhance their efficiency in various mobile and stationary applications by improving the ability of reversible storage of hydrogen [19]. As an example, the reduced rate of Mn, the simpler activation, and the decrease in the equilibrium pressure (for desorption, with 0.41 MPa to 0.26 MPa at 25 °C) with a marginally lower hysteresis (from 0.64 to 0.62 MPa) have all contributed to the Mn substitution's increased appeal in hydrides composition [62–64].

Therefore, in light of the previous findings, the current study investigates the hydrogen absorption isotherms for the compound  $\text{MmNi}_{4.2}\text{Mn}_{0.8}$  at different temperatures using both experimental and numerical methods. We decided to use a mathematical model grounded in statistical physics formalism [65]. This model has been widely used by researchers in the study of hydrogen storage processes [43,66–73]. The mathematical model expressions are susceptible to adjusting the experimental isotherms, making it possible to finely define the microscopic states of the absorption reaction. Thus, applying the statistical physics model to investigate the hydrogen absorption phenomenon is quite interesting. Firstly, as it contains in its expressions important physical parameters different from empirical models like Langmuir and Freundlich, whose parameters typically do not obtain a direct physical meaning that can be inferred from experimental data after a numerical simulation [66,67], the storage system can be investigated by determining the various physicochemical parameters related to the absorption phenomenon. Secondly, it provides a clear knowledge of the thermodynamic properties that control the evolution of the system during the absorption reaction, such as the reaction's internal energy and entropy. The absorption isotherms were thus simulated using empirical models based on theoretical and mathematical expressions, formalized within the framework of the grand canonical ensemble of statistical physics. In a recent study [67], we investigated the hydrogen absorption characteristics of the compounds  $\text{MmNi}_{4.6}\text{Fe}_{0.4}$  and  $\text{MmNi}_{4.6}\text{Al}_{0.4}$  using this model. In this study, we experimentally and numerically investigated the effect of Mn doping on hydrogen storage compounds' properties as a function of temperature and pressure. Thus, an intriguing hydrogen storage material,  $\text{MmNi}_{4.2}\text{Mn}_{0.8}$ , is reported in this study.

Such a model was used to calculate the energy coefficients ( $P_1, P_2$ ), the interstitial site densities ( $N_{m1}, N_{m2}$ ), and the number of atoms of hydrogen per site ( $n_1, n_2$ ). Relevantly, the parameters acquired were then be applied to ascertain the thermodynamic functions that characterize the metal's reactions to the absorption of hydrogen. Depending on the variations in pressure and temperature, the variation in hydrogen concentration per unit of metal ( $H/M$ ), the internal energy ( $E_{\text{int}}$ ), the Gibbs free energy, and entropy ( $S$ ) were be computed numerically and are discussed herein.

## 2. Equipment and Procedures

The Indian mixed metal Mm that was utilized has a typical composition of roughly 23% lanthanum, 18% neodymium, 43% cerium, 5% praseodymium, 8% iron, and 3% samarium. It was fused in an argon atmosphere with manganese and high-purity nickel (99.99%).

The volumetric method was used to measure hydrogen absorption isotherms [68]. Its principle is as follows: A metal hydrogen reactor (MHR) with high pressure was filled with 20 g of the prepared material and connected to a hydrogen tank of buffer volume via Swagelok valves and aluminum connection tubes. During absorption, the hydrogen tank was charged to the desired pressure ( $P_0$ ) and placed in contact with the reactor. The hydrogen pressure decreased in the tank until it reached an equilibrium value ( $P_{\text{eq}}$ ). A pressure sensor was installed within the hydride bed, coupled with an Agilent acquisition card and a microcomputer, allowing the control of the temporal evolution of the pressure of the absorbed hydrogen. The temperature inside the hydride bed was regulated by cooled water from a thermostatic bath through an external cylindrical heat exchanger (Figure 1).

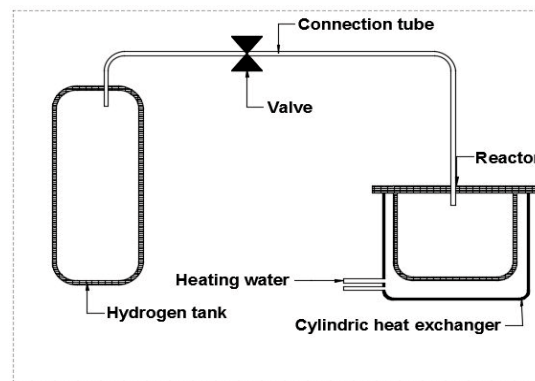


Figure 1. Experimental device.

### 3. Experimental Isotherms

Typically, P-C-T isotherms, which show the pressure–concentration–temperature records, are monitored to characterize a metal hydride system. Figure 2 presents the experimental isotherms of the absorption of hydrogen by  $\text{MmNi}_{4.2}\text{Mn}_{0.8}$  versus different temperatures.

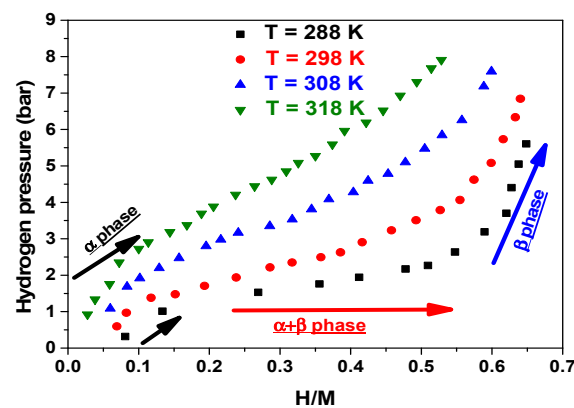


Figure 2. Absorption isotherms in the  $\text{MmNi}_{4.2}\text{Mn}_{0.8}$  compound at different temperatures.

The hydrogen capacity, i.e., concentration, is commonly expressed in terms of atoms of hydrogen per metal species, i.e., H/M. It is most effective to use its highest capacity  $[\text{H}/\text{M}]_{\text{max}}$  to characterize the metal hydride. The following could serve as a summary of the key findings pertaining to the acquired outcomes. It is seen from Figure 2 that at a given temperature, an isotherm is composed of three phases:

- \*  $\alpha$  phase: distinguished by a sharp rise in pressure against a slight change in H/M;
- \*  $\alpha + \beta$  phase: marked by a remarkable increase in H/M and a slight shift in pressure (equilibrium plateau);
- \*  $\beta$  phase: characterized by a stabilization of H/M against a rise in pressure.

Actually, atoms of hydrogen in the  $\alpha$  phase of the crystal lattice are in solid solution at low-hydrogen compositions. The system's hydrogen content affects the equilibrium pressure of this phase. As the temperature rises, the  $\alpha$ -phase saturation rate increases. Then, at higher hydrogen rates, a  $\alpha$ -phase structural transition gives rise to the  $\beta$  phase (rutile structure), a hydride with a specific composition. Constant pressure causes this transformation to occur. Thus, the presence of the phases  $\alpha$  and  $\beta$  together occurs on an equilibrium plateau up to a rate that is not too far from the  $\beta$  phase's saturation. The majority of the hydrogen is absorbed in the plateau region, with a slight change in pressure. This plate's pressure rises as its temperature does. Beyond this, saturating the  $\beta$  phase requires a significant increase in pressure. Thus, the amount of hydrogen absorbed above the plateau pressure is extremely small.

Therefore, a hydride storage material's equilibrium dissociation pressure ( $P_{eq}$ ) is one of its most crucial characteristics. According to Figure 2, if the temperature changes between 288 K and 318 K, the equilibrium plateau of the compound  $MmNi_{4.2}Mn_{0.8}$  is situated roughly between 2 bar and 5 bar. We must consider that, for instance, the equilibrium pressure of the compound  $MmNi_{4.2}Mn_{0.8}$  at 218 K (5 bar) is essentially half of that of the compound  $La_{0.91}Ce_{0.9}Ni_5$  (8 bars) at the same experimental conditions and practically of the same order of magnitude as that of  $LaNi_5$  (5 bar) [43]. Furthermore, the Mn-doped compound's equilibrium pressure is nearly half that of the  $MmNi_5$  compound [69]. Likewise, the Mn-doped compound is at roughly the same equilibrium plateau level as the compound  $MmNi_{4.6}Al_{0.4}$  and shows an equilibrium plateau drop that is roughly five times smaller than that of the Fe-doped compound [67]. In view of this,  $MmNi_{4.2}Mn_{0.8}$  is thought to have a lower and more promising equilibrium pressure. As a result, the compound presents the simple reversibility, cyclability, and stability of the hydride under cycling at room temperature.

Without a doubt, there is still less than one hydrogen atom for every metal unit. In comparison, at a given temperature, the Fe-doped compound has almost twice the H/M of the Mn-doped compound. For example, at 288 K, the  $MmNi_{4.2}Mn_{0.8}$  compound shows an [H/M] max of 0.6, while the compound  $MmNi_{4.6}Fe_{0.4}$  exhibits an [H/M] max of 1.2 [67].

#### 4. The Plot of Van't Hoff

Plotting the equilibrium pressure ( $P_{eq}$ ) versus the reciprocal of the absolute temperature ( $1/T$ ) is referred to as the van't Hoff plot. The standard enthalpy ( $\Delta H_0$ ) and entropy ( $\Delta S_0$ ) of the reaction can be determined using the slope and the intercept of the plot, as shown in the van't Hoff equation [70]:

$$\ln\left(\frac{P_0}{P_{eq}}\right) = \frac{\Delta H_0}{RT} - \frac{\Delta S_0}{R} \quad (1)$$

where  $T$  is the absolute temperature,  $R$  is the constant of ideal gas, and  $P_0$  is the standard pressure, which is usually taken to be 1 atm. Figure 3 presents the van't Hoff plot corresponding to  $MmNi_{4.2}Mn_{0.8}$  at the investigated temperature.

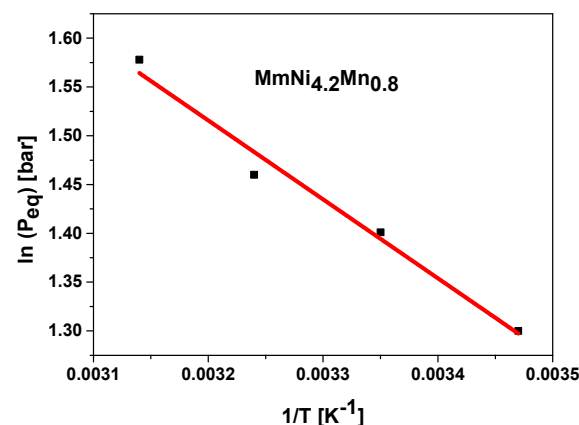


Figure 3. The plot of van't Hoff.

The absorption reaction's enthalpy and entropy are then inferred from the plot. Table 1 provides their values.

Table 1. The absorption reaction's enthalpy and entropy values.

| $\Delta H_0$ (kJ mol <sup>-1</sup> ) | $\Delta S_0$ (J mol <sup>-1</sup> K <sup>-1</sup> ) |
|--------------------------------------|---|
| -12.4                                | -81.18  |

The quantity of heat that is let out during the absorption of hydrogen and that must be supplied again during desorption is determined by the formation enthalpy. This value is in good agreement with that of type-AB<sub>5</sub> alloys [71]. The fact that  $\Delta H$  is negative indicates that the reaction of absorption is exothermic, as the hydride bed system releases heat during this process. Also,  $\Delta S$  decreases as a result of the change from a more disordered gaseous state (gaseous hydrogen) to a more ordered solid state (hydride), as indicated by the negative value of entropy.

## 5. Modelling

### 5.1. Introduction of the Model

The double-energy mono-layer model with two types of sites is a mathematical model developed by statistical physics. Thus, it is the most stable among the statistical physics-based numerical models since it most closely matches the experimental absorption data, as indicated by Bouaziz N. et al. [72]. Therefore, this model was used in the present study. When using a model, a number of considerations and assumptions must be made [73]. Firstly, hydrogen must be considered an ideal gas (at low pressure). Moreover, we must only consider the two most important degrees of freedom for atoms: translation with a typical translational temperature of  $\varphi_{tr} = 10^{-15}$  K and rotation with a typical rotational temperature of  $\varphi_{rot} = 85.3$  K. Furthermore, remember that a varying amount of  $n_a$  atoms of hydrogen is stored in  $N_m$  interstitial sites spaced across the unit mass of the absorbent material. Thereby, the equation describing the reversible hydrogen storage reaction in the metal is as follows (Equation (2)):



In the following reaction, M presents the hydrogen storage material, n presents the stoichiometric coefficient, and  $MH_n$  presents the formed hydride. Moreover, the hydrogen atoms in metal alloys can be viewed as aggregated in ( $H_n$ ).

Since the sorption process involves a transfer of particles from the state of freedom to the absorption state, the grand canonical ensemble must be utilized to study it (Equation (3)):

$$Z_{gc} = \sum_{N_j} e^{-\beta(-\epsilon_j - \mu)N_j} \quad (3)$$

where  $N_j$ , the occupation state of the receptor sites, is either equal to 0 or 1;  $-(-\epsilon_j)$  denotes the absorption energy at the receptor sites;  $\mu$ , the absorbed site's chemical potential, is equivalent to  $1/(k_B T)$ , where  $k_B$  denotes the Boltzmann constant. The system's microscopic states are defined by the grand canonical partition function ( $Z_{gc}$ ) in relation to the physical circumstances in which it is situated. Given that, the  $N_m$  receptor sites per mass unit are linked to the total grand canonical partition function. In the event that these sites are considered to be independent and identical,  $Z_{gc}$  can be represented as a simple product (Equation (4)):

$$Z_{gc} = \prod_j (Z_{gc})^{N_{jm}} \quad (4)$$

As a result, two atoms of hydrogen,  $N_1$  and  $N_2$ , are stored in two distinct types of interstitial sites ( $n_1$  and  $n_2$ ) in the monolayer model with two energies. The density in the first category of sites is  $N_{m1}$ , while the density in the second category is  $N_{m2}$ . The energies  $\epsilon_1$  and  $\epsilon_2$ , respectively, define them. Under these circumstances,  $Z_{gc}$  can be written as (Equation (5)):

$$Z_{gc} = (z_{1gc})^{N_{1m}} \times (z_{2gc})^{N_{2m}} \quad (5)$$

$Z_{gc}$  of the first and second site types are denoted by  $Z_{1gc}$  and  $Z_{2gc}$ , respectively:

$$z_{1gc} = \sum_{N_j=0,1} e^{\frac{(-\epsilon_1-\mu)N_j}{k_B T}} = 1 + e^{\beta(\epsilon_1+\mu)} \quad (6)$$

$$z_{2gc} = \sum_{N_j=0,1} e^{\frac{(-\epsilon_2-\mu)N_j}{k_B T}} = 1 + e^{\beta(\epsilon_2+\mu)} \quad (7)$$

The chemical potential of an individual free dihydrogen molecule is expressed in the gaseous form as (Equation (8)):

$$\mu_m = \mu/n = k_B T \ln\left(\frac{N}{Z_{gc}}\right) \quad (8)$$

where  $\mu$  represents the chemical potential of the interstitial site, and  $n$  denotes the number of atoms per site.  $Z_{gc}$  can be expressed as follows (Equation (9)):

$$z_{gc} = z_{gtr} \times z_{grot} = V \left(\frac{2\pi m k_B T}{h^2}\right)^{3/2} * \frac{T}{2\theta_{rot}} \quad (9)$$

where  $Z_{grot}$  and  $Z_{gtr}$  stand for the translation and rotation partition functions, respectively. The parameters of the system are as follows:  $m$  is the mass of a hydrogen atom,  $V$  is its volume,  $h$  is Planck's constant ( $h = 6.6260 \times 10^{-34}$  m<sup>2</sup> kg/s), and  $\theta_{rot}$  is the dihydrogen molecule's characteristic rotational temperature. For an ideal hydrogen gas,  $z_{gtr}$  can be expressed using the expression in relation to the saturated vapor pressure  $P_{VS}$  and the vaporization energy ( $\Delta E_v$ ) as follows (Equation (10)):

$$Z_{gtr} = \beta P_{vs} e^{\Delta E_v} z_{gtr} = \beta P_{vs} e^{\frac{\Delta E_v}{RT}} \quad (10)$$

where

$$P_{VS} = \left(\frac{2\pi K_B T}{h^2}\right)^{\frac{3}{2}} K_B T e^{-\frac{\Delta E_v}{RT}} \quad (11)$$

Therefore, using Equation (2), the following formulae yield the average numbers of occupied sites (Equation(12)):

$$N_O = n_1 N_{01} + n_2 N_{02} = n_1 \frac{N_{1m}}{1 + \left(\frac{P_1}{P}\right)^{n_1}} + n_2 \frac{N_{2m}}{1 + \left(\frac{P_2}{P}\right)^{n_2}} \quad (12)$$

where  $P_1 = K_B T Z_g e^{-1m}$  and  $P_2 = K_B T Z_g e^{-2m}$  are the saturation pressures in the middle, which identify the first and second site types, respectively.

We must consider that the amounts that are experimentally stored are expressed in terms of H/M or the number of H atoms per unit formula. Thereby, for every type of site, the absorbed amount is equal to (Equation (13)):

$$\left[\frac{H}{M}\right]_1 = \frac{n_1 N_{1m}}{(N_{1m} + N_{2m}) \left(1 + \left(\frac{P_1}{P}\right)^{\left(\frac{n_1}{2}\right)}\right)} = \frac{\left[\frac{H}{M}\right]_{1sat}}{1 + \left(\frac{P_1}{P}\right)^{\left(\frac{n_1}{2}\right)}} \quad (13)$$

$$\left[\frac{H}{M}\right]_2 = \frac{n_2 N_{2m}}{(N_{1m} + N_{2m}) \left(1 + \left(\frac{P_2}{P}\right)^{\left(\frac{n_2}{2}\right)}\right)} = \frac{\left[\frac{H}{M}\right]_{2sat}}{1 + \left(\frac{P_2}{P}\right)^{\left(\frac{n_2}{2}\right)}} \quad (14)$$

with

$$\left[\frac{H}{M}\right] = \left[\frac{H}{M}\right]_1 + \left[\frac{H}{M}\right]_2 \quad \text{and} \quad \left[\frac{H}{M}\right]_{sat} = \left[\frac{H}{M}\right]_{1sat} + \left[\frac{H}{M}\right]_{2sat}$$

Subsequently, the following defines the equation for the total quantity absorbed or desorbed per unit formula:

$$\left[\frac{H}{M}\right] = \frac{\left[\frac{H}{M}\right]_{1sat}}{1 + \left(\frac{P_1}{P}\right)^{\left(\frac{n_1}{2}\right)}} + \frac{\left[\frac{H}{M}\right]_{2sat}}{1 + \left(\frac{P_2}{P}\right)^{\left(\frac{n_2}{2}\right)}} \quad (15)$$

In order to interpret the absorption process, six fitted parameters were determined for this model: the atoms numbers per site for each type ( $n_1$ ,  $n_2$ ), their densities of ( $N_{m1}$ ,  $N_{m2}$ ), and the pressures at middle saturation ( $P_1$  and  $P_2$ ).

Note: Absorption involves the penetration of hydrogen atoms into the volume of the storage material, while adsorption is the state that occurs on the surface of the substrate. Several studies have considered that absorption and adsorption are energetically similar since both mechanisms belong to the same category of diffusional equilibrium phenomena. Thus, several researchers have shown that the double-energy mono-layer model is suitable with excellence for studying the phenomenon of hydrogen absorption by metal hydrides [71–73].

### 5.2. Adjustment of the Experimental P-C-T

Using the model previously described, the hydrogen absorption isotherms were adjusted. The adjustment demonstrates that the suggested model and the experimental data agree perfectly (Figure 4).

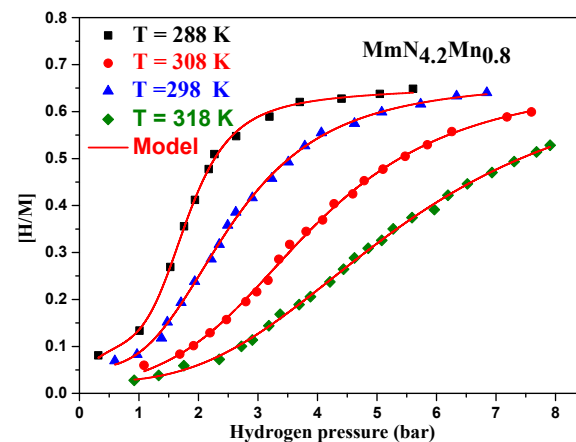


**Figure 4.** Fitting of the absorption isotherms using the double-energy mono-layer model.

Depending on the model selected, we can explain the development of the two distinct phases: a first hydride solid solution, which is thought to be phase  $\alpha$ , and a second hydride phase, which is thought to be phase  $\beta$ . As a result, the two-energy mono-layer model that was employed to fit the experimental data makes the reaction easier to study and accurately depicts how hydrogen is reversibly stored by the compound. Table 2 displays the values of the fitting parameters versus temperature during the absorption and desorption processes.

**Table 2.** Fitting parameters for the  $\text{MmNi}_{4.2}\text{Mn}_{0.8}$  compound for the hydrogen absorption versus temperature.

| Temperature (K) | Absorption Process |       |      |        |        |       |       |
|-----------------|--------------------|-------|------|--------|--------|-------|-------|
|                 | $n_1$              | $n_2$ | $n$  | $Nm_1$ | $Nm_2$ | $P_1$ | $P_2$ |
| 288             | 0.57               | 4.96  | 2.76 | 0.39   | 0.096  | 1.05  | 1.8   |
| 298             | 1.05               | 3.63  | 2.34 | 0.12   | 0.16   | 2.47  | 3.99  |
| 308             | 0.12               | 3.12  | 1.62 | 0.73   | 0.19   | 0.04  | 2.55  |
| 318             | 0.093              | 2.9   | 1.49 | 0.54   | 0.22   | 1.01  | 5.43  |

Prior to being utilized to determine the thermodynamic functions characterizing the hydrogen storing reaction, such as Gibbs free energy, the internal energy, and entropy, these parameters will be examined as a function of temperature.

### 5.3. Numerical Findings

#### 5.3.1. Temperature's Effect on $n_1$ , $n_2$ , and $n$

The number of sites available for hydrogen storage in hydride form and temperature have a complex relationship that depends on the particulars of the hydride material. The statistical physics model proposed for modeling the hydrogen storage in  $\text{MmNi}_{4.2}\text{Mn}_{0.8}$  requires the existence of two types of interstitial sites to receive or release hydrogen atoms during absorption or desorption. In these circumstances, Equation (1) can be viewed as the sum of the following two equations that show the contributions of  $n_1$  and  $n_2$ , which represent the number of hydrogen atoms in the first and second types of sites, respectively:



From Equations (1) and (12), it can be deduced that  $n$  can be expressed as follows:

$$n = \frac{n_1 + n_2}{2} \quad (19)$$

The variables  $n_1$ ,  $n_2$ , and  $n$  are given in Figure 5.

As seen, the two kinds of sites behave differently depending on temperature and do not have the same order of magnitude. Firstly, the result is  $n_1 < n_2$ . The distinction in size between the first-phase and second-phase sites could provide justification for this aspect.

Then, it is shown that, as the temperature rose from 288 K to 298 K, there were more hydrogen atoms in the first type of site  $n_1$ . A decrease in the quantity of hydrogen atoms in the second class of sites ( $n_2$ ) offsets this increase. Afterward, the quantity of hydrogen atoms in the two types of sites decreases as the temperature rises. As an outcome,  $n$  decreases linearly as a result of  $n_1$  and  $n_2$ 's reactions to the temperature increase. The exothermic character of the reaction of hydrogen absorption explains the decrease in  $n$  with temperature. As a result, as demonstrated, the rise in temperature blocks the interstitial receptor sites for hydrogen atoms, which typically results in a hindrance to the absorption reaction. Another point that needs to be noted is that since  $n$  is still greater than 1, it is evident that there are multiple hydrogen atoms at each site. This suggests that the interstitial sites of the metal matrix experience a phenomenon of hydrogen atom agglomeration.

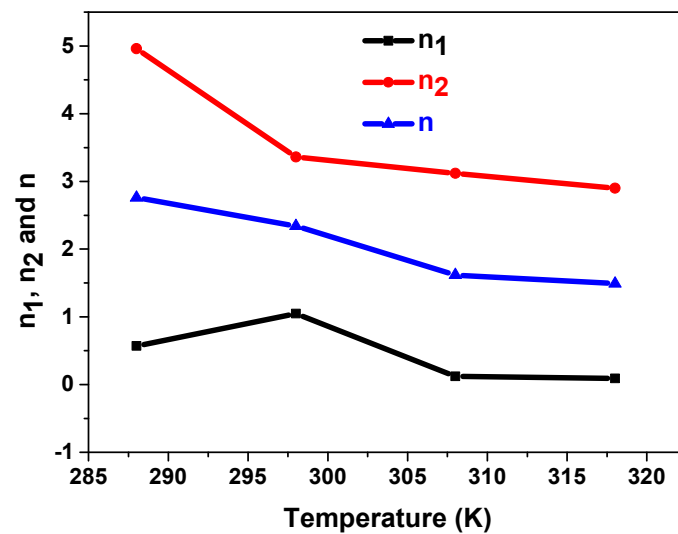


**Figure 5.** Dependence of  $n_1$ ,  $n_2$ , and  $n$  on temperature during hydrogen absorption in the compound  $MmNi_{4.2}Mn_{0.8}$ .

### 5.3.2. Temperature's Influence on Interstitial Site Densities $N_{m1}$ and $N_{m2}$

For sites type 1 and type 2,  $N_{m1}$  and  $N_{m2}$  reveal the site number actually needed to absorb the number of atoms at saturation. Figure 6 depicts the temperature dependence of  $N_{m1}$  and  $N_{m2}$ .

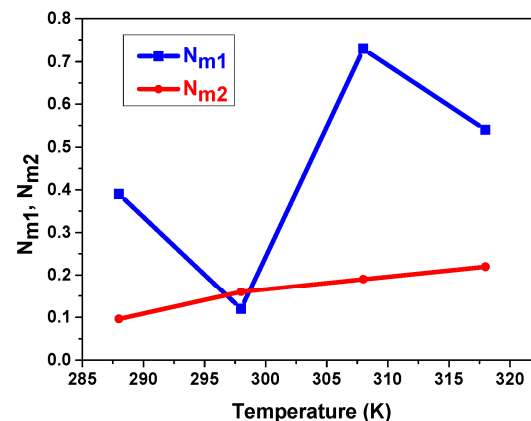


**Figure 6.** Dependence of  $N_{m1}$  and  $N_{m2}$  on temperature during hydrogen absorption in the compound  $MmNi_{4.2}Mn_{0.8}$ .

Firstly, it is shown that during absorption,  $N_{m1} > N_{m2}$ . This indicates that there are more sites in the first phase than in the second phase of the crystalline lattice of the  $MmNi_{4.2}Mn_{0.8}$  hydride. Secondly, it is demonstrated that  $N_{m1}$  and  $N_{m2}$  interact differently depending on the temperature. Therefore, a notable fluctuation of  $N_{m1}$  is observed despite the fact that the variation of  $N_{m2}$  with temperature is limited. This may lead to pulverization and degradation, potentially destroying the hydride's metal matrix. In fact, the simple destructibility of the substrate's surface brought on by volume expansion and the fragility of metal alloys are the main causes of their degradation. As a result, considerable fracturing, an intense gradient generating defects from the sample's surface towards the mass, and some cracks on the alloy's surface are seen during hydrogen absorption [73].

### 5.3.3. Temperature's Influence on $[H/M]_{1sat}$ and $[H/M]_{2sat}$

As previously demonstrated (Equation (12)) using the proposed model, the total absorption can be analyzed by two distinct contributions. Therefore, for the first and

second types of sites, the absorbed amounts per unit formula at saturation are determined by  $(n_1, N_{m1})$  and  $(n_2, N_{m2})$ , respectively, as follows:

$$\left[\frac{H}{M}\right]_{1sat} = \frac{n_1 N_{m1}}{N_{m1} + N_{m2}} \quad (20)$$

$$\left[\frac{H}{M}\right]_{2sat} = \frac{n_2 N_{m2}}{N_{m1} + N_{m2}} \quad (21)$$

The evolution of  $[H/M]_{1sat}$ ,  $[H/M]_{2sat}$ , and  $[H/M]_{sat}$  of the absorption reaction depending on temperature is depicted in Figure 7.

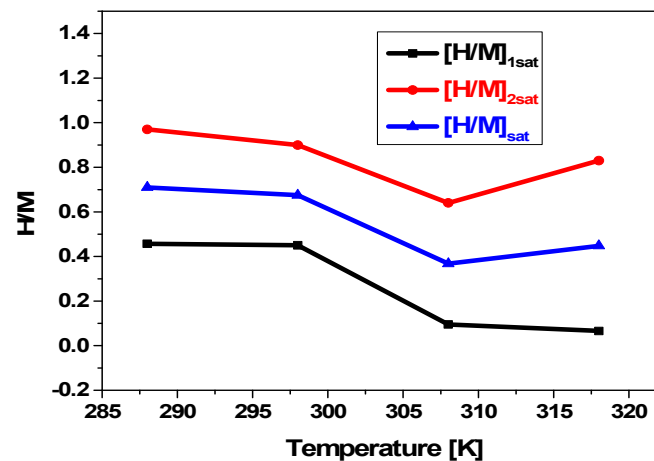


Figure 7. Dependence of  $[H/M]_{1sat}$ ,  $[H/M]_{2sat}$ , and  $[H/M]_{sat}$  on temperature during hydrogen absorption in the compound  $MmNi_{4.2}Mn_{0.8}$ .

First,  $[H/M]_{1sat} < [H/M]_{2sat}$  is demonstrated. The fact that  $n_2 > n_1$  explains this.

Then, for both kinds of sites, it is obvious that as temperature rises, the maximum amount of hydrogen absorbed falls. Consequently, the absorption process is exothermic for both kinds of sites as well as for the global system marked by  $[H/M]$ . Thus, thermal agitation is the cause of these variations. The experimental values (Figure 1) and the numerical values (Figure 7) of  $[H/M]$  as a function of temperature agree exactly.

#### 5.3.4. Temperature's Influence on the $\Delta E^1$ and $\Delta E^2$

The heat of absorption can be used to describe hydrogen absorption energies. These parameters are critical in determining the nature of the interaction between hydrogen and the  $MmNi_{4.2}Mn_{0.8}$  compound. The energies of hydrogen absorption ( $\Delta E^1$  and  $\Delta E^2$ ) for each type of site were calculated using the following formula:

$$\Delta E^1 = RT \ln\left(\frac{P}{P_1}\right) \quad (22)$$

$$\Delta E^2 = RT \ln\left(\frac{P}{P_2}\right) \quad (23)$$

where  $P$  is expressed in the following format:

$$P = \exp\left[12.69 - \frac{94.896}{T} + (1.1125) \ln(T) + (3.2915 \times 10^{-4}) T^2\right] \quad (24)$$

According to Figure 8, which depicts the relationship between the temperature and the energies of absorption, both  $\Delta E^1$  and  $\Delta E^2$  rise nearly linearly with rising temperatures with nearly equal values. This implies that at higher temperatures, greater pressure is needed for hydrogen to be transferred from the gaseous form to the absorbed phase. This

is consistent with the hydrogen absorption reaction's exothermic nature. This is explained by the absorption reaction's exothermic character. Moreover, the calculated energies range between 107 and 137 KJ/mol. This demonstrates that hydrogen atoms are chemically bound to the two types of receptor sites. The difference in  $\Delta E^1$  and  $\Delta E^2$  is the root cause of the difference in the first and second type of site sizes.

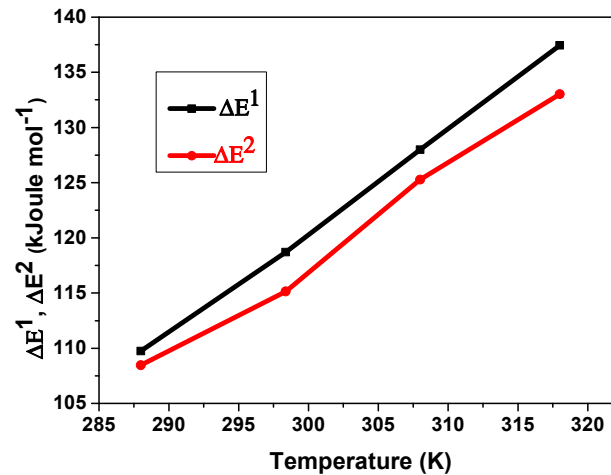


**Figure 8.** Dependence of  $\Delta E^1$  and  $\Delta E^2$  on temperature during hydrogen absorption in the compound  $MmNi_{4.2}Mn_{0.8}$ .

### 5.3.5. Variation in Hydrogen Concentration [H/M] with Pressure at Different Temperatures

Pressure affects the process of hydrogen absorption significantly, just like temperature does. It is one of the most important factors to take into account when developing and perfecting hydrogen storage systems. The [H/M] variation as a function of applied pressure versus temperature is shown in Figure 9.

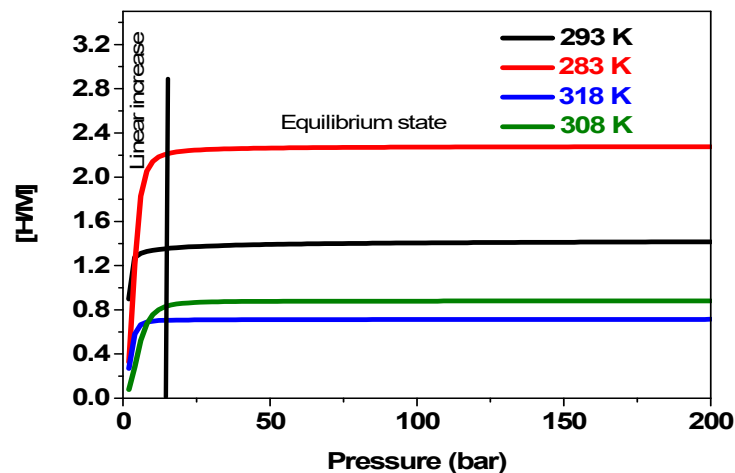


**Figure 9.** Variation of [H/M] depending on the applied pressure at 283 K, 293 K, 308 K, and 318 K.

As a starting point, we find from Figure 9 that raising the initial temperature decreases both the kinetics of the reaction and the amount of hydrogen absorbed, resulting in a less efficient reaction since the absorption reaction is exothermic. For instance, the maximum concentration of hydrogen per unit of metal decreases by about three times when the temperature rises from 288 k to 318 k. Additionally, it is demonstrated that at a given temperature, until the stabilization that occurs in the equilibrium state, the absorbed amount increases gradually depending on pressure. Therefore, hydrogen molecules occupy an increasing number of sites on the material as the pressure rises. The maximum amount

of hydrogen that can be adsorbed, denoted by  $[H/M]_{\max}$ , is typically the upper limit. The absorption process may get close to saturation, and the amount of hydrogen adsorbed may stabilize or plateau at higher pressures. When the pressure no longer significantly increases the amount of hydrogen adsorbed, the equilibrium state is reached.

### 5.3.6. Effects of Pressure on the System's Internal Energy Variation $U_{\text{int}}$ versus Temperatures

The total energy present in a system is represented by internal energy, i.e.,  $U_{\text{int}}$ , a fundamental and comprehensive function. It consists of potential energy, which is stored energy dependent on position or state, as well as kinetic energy, which is the energy of motion. The internal energy of a system is greatly influenced by its temperature and pressure. The following is the expression for the internal energy of hydrogen absorption [68]:

$$U_{\text{int}} = -\frac{\partial \ln(z_{gc})}{\partial \beta} + \frac{\mu}{\beta} \left( \frac{\partial \ln(z_{gc})}{\partial \mu} \right) \quad (25)$$

with

$$\mu = K_B T \ln \left( \frac{\beta P}{z_g} \right) \quad (26)$$

Consequently,  $U_{\text{int}}$  can be expressed in the following manner:

$$U_{\text{int}} = k_B \ln \left( \frac{\beta P}{z_g} \right) \left( \frac{N_{1m} \left( \frac{P}{P_1} \right)^{n_1}}{1 + \left( \frac{P}{P_1} \right)^{n_1}} + \frac{N_{2m} \left( \frac{P}{P_2} \right)^{n_2}}{1 + \left( \frac{P}{P_2} \right)^{n_2}} \right) - k_B T \left( \frac{N_{1m} \left( \frac{P}{P_1} \right)^{n_1}}{1 + \left( \frac{P}{P_1} \right)^{n_1}} + \frac{N_{2m} \left( \frac{P}{P_2} \right)^{n_2}}{1 + \left( \frac{P}{P_2} \right)^{n_2}} \right) \quad (27)$$

The variation of  $U_{\text{int}}$  depending on pressure versus various temperatures during the reaction of hydrogen absorption by the  $\text{MmNi}_{4.2}\text{Mn}_{0.8}$  compound is shown in Figure 10.

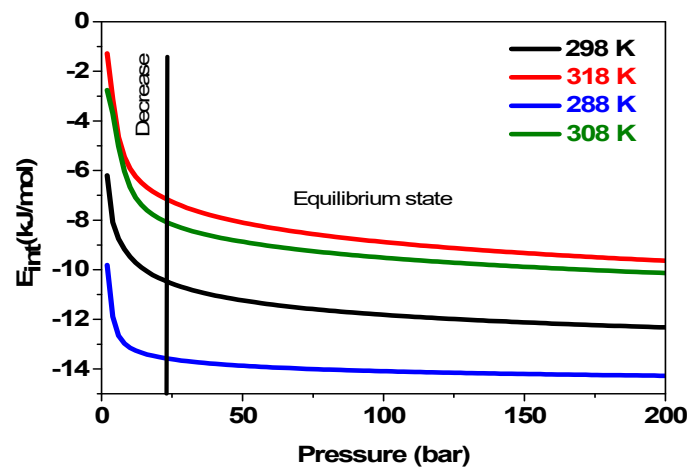


Figure 10. Variation of the  $U_{\text{int}}$  depending on the applied pressure at 283 K, 293 K, 308 K, and 318 K.

Firstly, it is shown from Figure 10 that the system must supply energy since the internal energy values are negative, which prevents hydrogen atoms from being absorbed. This indicates that the process of absorption is exothermic. This clarifies why the system's internal energy increases as a result of the initial temperature rising. For instance, the energy dissipated at 288 K is seven times less than that required to be supplied at 318 K. Moreover, it is noted that as pressure rises, the values of the internal absorption energies decrease. This suggests that at high pressure, the system can absorb hydrogen with less energy.

### 5.3.7. Effects of Pressure on the System's Entropy Variation versus Temperatures

Entropy is a thermodynamic function that quantifies the level of disorder or randomness in a system both prior to and following a chemical reaction. It shows how the system's energy and matter distribution have changed. The grand potential and the absorption entropy are related by the following relationships:

$$J = -K_B T \ln(z_{gc}) \quad (28)$$

$$J = -\frac{\partial \ln(z_{gc})}{\partial \beta} - TS_a \quad (29)$$

$$TS_a = -\frac{\partial \ln(z_{gc})}{\partial \beta} + K_B T \ln(z_{gc}) \quad (30)$$

Consequently, the entropy of the absorption  $S_a$  can be defined using the fitted parameters in this way:

$$S_a = -k_B \left( N_{1m} \ln \left( 1 + \left( \frac{P}{P_1} \right)^{n_1} \right) + N_{2m} \ln \left( 1 + \left( \frac{P}{P_2} \right)^{n_2} \right) \right) - \left( \frac{N_{1m} \left( \frac{P}{P_1} \right)^{n_1} \ln \left( \frac{P}{P_1} \right)^{n_1}}{1 + \left( \frac{P}{P_1} \right)^{n_1}} + \frac{N_{2m} \left( \frac{P}{P_2} \right)^{n_2} \ln \left( \frac{P}{P_2} \right)^{n_2}}{1 + \left( \frac{P}{P_2} \right)^{n_2}} \right) \quad (31)$$

Figure 11 presents the entropy variation of the reaction of absorption by the  $MmNi_{4.2}Mn_{0.8}$  compound depending on pressure versus different temperatures.

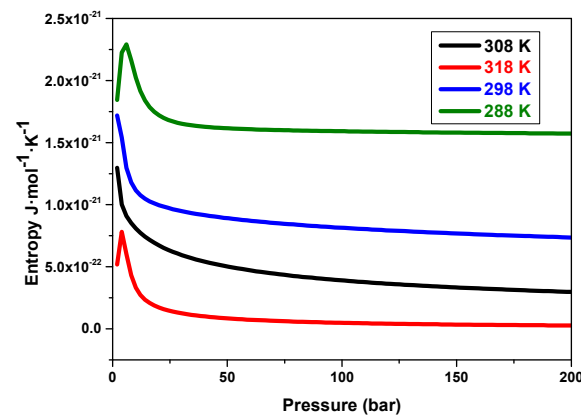


Figure 11. Variation of the entropy depending on the applied pressure for different temperatures.

The findings demonstrated that, at a specific temperature, the absorption reaction's entropy crosses a maximum (a pic). Throughout the absorption reaction, the disorder progressively rises, reaches its highest point near the equilibrium state, and then eventually drops and maintains stability, indicating that the reaction has attained its state of equilibrium. The entropy's maximum is found to decrease with rising temperatures. This can be attributed to the endothermic character of the reaction.

### 5.3.8. Effects of Pressure on the Gibbs Variation versus Temperatures

The Gibbs free energy is expressed as follows:

$$G_a = \mu \times n \times N_0 = \mu \left[ \frac{H}{M} \right]_0 \quad (32)$$

As a result,  $G_a$  is written depending on the fitted parameters as given below:

$$G_a = K_B \ln \left[ \frac{\beta P}{z_g} \left( \frac{n_1 N_{1m}}{1 + \left(\frac{P_1}{P}\right)^{\left(\frac{n_1}{2}\right)}} + \frac{n_2 N_{2m}}{1 + \left(\frac{P_2}{P}\right)^{\left(\frac{n_2}{2}\right)}} \right) \right] \quad (33)$$

The Gibbs variation versus pressure at various temperatures during hydrogen absorption by the  $\text{MmNi}_{4.2}\text{Mn}_{0.8}$  compound is shown in Figure 12.

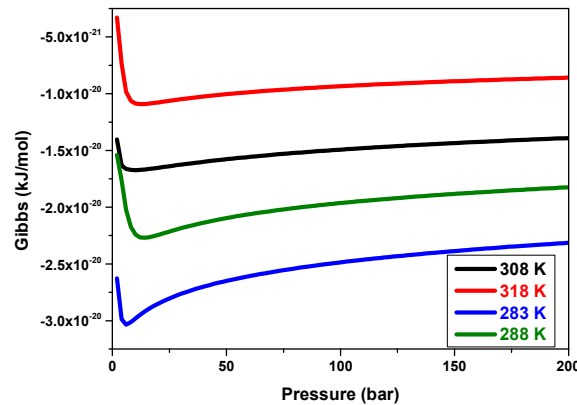


**Figure 12.** Gibbs free energy evolution for  $\text{MmNi}_{4.2}\text{Mn}_{0.8}$  at various temperatures as a function of pressure.

Firstly, the absorption phenomenon appears to be thermodynamically spontaneous in nature, as indicated by the negative values of the Gibbs energy. Then, as the temperature rises, the free enthalpy values rise as well, indicating that absorption is less likely to occur at high temperatures. The temperature makes it impossible for the absorption mechanism to be accomplished.

Note: Entropy and Gibbs free energy infer directly about the variation of the enthalpy  $H$  since the enthalpy change is the sum of the Gibbs free energy change and the product of the absolute temperature times the entropy change.

## 6. Conclusions

This article examined the properties of hydrogen absorption by the compound  $\text{MmNi}_{4.2}\text{Mn}_{0.8}$  through both experimental and numerical modeling. Firstly, it was demonstrated by experimental hydrogen absorption isotherms that a lower and more promising equilibrium pressure results from doping Ni with Mn. This thus demonstrates the fundamental properties of cyclability, hydride stability, and simple reversibility under cycling at room temperature. Then, the experimental results were compared to a numerical model based on the formalism of statistical physics. Therefore, the characteristics of steric and energetic factors implicated in the hydrogen absorption reaction, including  $(n_1, n_2)$ ,  $(N_{m1}, N_{m2})$ , and  $(P_1, P_2)$ , were determined and discussed depending on the temperature thanks to the perfect agreement between the experimental and numerical data. Ultimately, these parameters were utilized to translate a microscopic description of the absorption process into macroscopic characteristics. Consequently, the heat of the absorption reaction and the concentration of hydrogen atoms per unit of hydride were calculated. In addition, the three thermodynamic entropy, internal energy, and Gibbs free energy functions that control the hydrogenation process were measured and examined according to pressure variation at various operating temperatures. The results showed that increasing the temperature blocks the interstitial receptor sites  $n$  for hydrogen atoms, which generally results in an obstacle to the absorption reaction. Although the literature already contains the experimental outcomes, the theoretical instrument displays its resilience in characterizing the compound's process of absorbing hydrogen.

**Author Contributions:** Methodology, S.B. and A.J.; Validation, S.B. and M.H.D.; Formal analysis, A.A., C.B. and S.M.A.; Investigation, S.B.; Writing—original draft, A.A. and M.H.D.; Writing—review & editing, S.M.A. and M.H.D.; Supervision, A.J.; Funding acquisition, A.A. and S.M.A. All authors have read and agreed to the published version of the manuscript.

**Funding:** This research received no external funding.

**Institutional Review Board Statement:** Not applicable.

**Informed Consent Statement:** Not applicable.

**Data Availability Statement:** Data are contained within the article.

**Acknowledgments:** The Researchers would like to thank the Deanship of Graduate Studies and Scientific Research at Qassim University for financial support (QU-APC-2024-9/1).

**Conflicts of Interest:** The authors declare no conflict of interest.

## References

1. Yi, X.; Fang, Z. Impact of energy depletion, human development, and income distribution on natural resource sustainability. *Resour. Policy* **2023**, *83*, 103531.
2. Iñaki, A.; Iñigo, C.P.; Rosa, L.; Gorka, B.; Roberto, B. The energy requirements of a developed world. *Energy Sustain. Dev.* **2016**, *33*, 1–13.
3. Françoise, B.; Mara, M.; Alfredo, C.; Philipp, B.; Veneta, K. Sustainable energy transitions and social inequalities in energy access: A relational comparison of capabilities in three European countries. *Glob. Transit.* **2019**, *1*, 226–240.
4. Oguz, O.Y. World energy outlook and state of renewable energy: 10-Year evaluation. *Innov. Green Dev.* **2023**, *2*, 100070.
5. Shiqi, Z.; Yupeng, W.; Xiaoqiang, G.; Zheng, L.; Xiaofei, S.; Frede, B. Overview of US patents for energy management of renewable energy systems with hydrogen. *Int. J. Hydrogen Energy* **2023**, *48*, 9574–9591.
6. Joan, B.B.; Elisa, T.B. Impacts of intermittent renewable generation on electricity system costs. *Energy Policy* **2016**, *94*, 411–420.
7. Chu, D.I.; Samuel, G.; Emmanuel, T.; Eric, E.D. Distributed Generation and Renewable Energy Integration into the Grid: Prerequisites, Push Factors, Practical Options, Issues and Merits. *Energies* **2021**, *14*, 5375.
8. Antonio, S.; Qi, Z.; Mariano, M.; Pastora, V. Towards a new renewable power system using energy storage: An economic and social analysis. *Energy Convers. Manag.* **2022**, *252*, 115056.
9. Fan, Z.; Pengcheng, Z.; Meng, N.; Jon, M. The survey of key technologies in hydrogen energy storage. *Int. J. Hydrogen Energy* **2016**, *41*, 14535–14552.
10. Alka, P.; Rekha, D.; Jyoti, G.; Jyothi, C.; Vivek, A.; Pramod, H.B. Insights into renewable hydrogen energy: Recent advances and prospects. *Mater. Sci. Energy Technol.* **2020**, *3*, 319–327.
11. Meiling, Y.; Hugo, L.; Elodie, P.; Robin, R.; Samir, J.; Daniel, H. Hydrogen energy systems: A critical review of technologies, applications, trends and challenges. *Renew. Sustain. Energy Rev.* **2021**, *146*, 111180.
12. Ujwal, S.M.; Nidhi, B.; Aditi, P.; Subramanya, K.N.; Lourdu, A.R. Challenges associated with hydrogen storage systems due to the hydrogen embrittlement of high strength steels. *Int. J. Hydrogen Energy* **2023**, *47*, 17894–17913.
13. Ahmed, O.; Neha, N.; Ahmed, M.E.; Mahmoud, H.; Amer, A.H.; Ala'a, H.A.M.; David, W.R. Hydrogen production, storage, utilisation and environmental impacts: A review. *Environ. Chem. Lett.* **2022**, *20*, 153–188.
14. Nejc, K.; Ilena, G.; Franz, W.; Markus, S.; Alexander, T. A review on metal hydride materials for hydrogen storage. *J. Energy Storage* **2023**, *72*, 108456.
15. Hoffman, K.C.; Reilly, J.J.; Salzano, F.J.; Waide, C.H.; Wiswall, R.H.; Winsche, W.E. Metal hydride storage for mobile and stationary applications. *Int. J. Hydrogen Energy* **1976**, *1*, 133–151. [[CrossRef](#)]
16. Mykhalo, V.L.; Ivan, T.; Moegamat, W.D.; Yevgeniy, V.K.; Adrian, P.; Dana, S.; Righardt, E.; Gerhard, L.; Vladimir, L. Metal hydride hydrogen storage and supply systems for electric forklift with low-temperature proton exchange membrane fuel cell power module. *Int. J. Hydrogen Energy* **2016**, *41*, 13831–13842.
17. Inga, B.; Marc, L. Operation strategies for gas solid reactions in thermal energy storage systems. *J. Energy Storage* **2021**, *40*, 102767.
18. Stefan, B.; Ratnesh, T.; Amir, S.; Michael, O. Heat/mass transfer enhancement of an exothermic absorption utilizing a spinning disk reactor. *Int. J. Heat Mass Transf.* **2019**, *129*, 326–341.
19. Hassan, I.A.; Haitham, S.R.; Mohamed, A.S.; Daniel, H. Hydrogen storage technologies for stationary and mobile applications: Review, analysis and perspectives. *Renew. Sustain. Energy Rev.* **2021**, *149*, 111311. [[CrossRef](#)]
20. Yuanlu, L.; Erika, T.; Fernando, Z.; Verónica, D. Design of a AB<sub>5</sub>-metal hydride cylindrical tank for hydrogen storage. *Int. J. Hydrogen Energy* **2021**, *46*, 33889–33898.
21. Jean-Marc, J.; Valérie, P.-B.; Fermin, C.; Junxian, Z.; Michel, L. LaNi<sub>5</sub> related AB<sub>5</sub> compounds: Structure, properties and applications. *J. Alloys Compd.* **2021**, *862*, 158163.
22. Mahvash, A.; Rohit, M.; Pratibha, S. Heat transfer techniques in metal hydride hydrogen storage: A review. *Int. J. Hydrogen Energy* **2017**, *42*, 30661–30682.
23. Joakim, A.; Stefan, G. Large-scale storage of hydrogen. *Int. J. Hydrogen Energy* **2019**, *44*, 11901–11919.

24. Liang, L.; Alexander, I.; Daniel, L.; Ashleigh, C.; Wendy, T.; Cherry, C.; Jon, Y.; Liezl, S. Metal Hydride Composite Structures for Improved Heat Transfer and Stability for Hydrogen Storage and Compression Applications. *Inorganics* **2023**, *11*, 181.
25. Belkhiria, S.; Briki, C.; Dhaou, M.H.; Alresheedi, F.; Jemni, A. A study of the magnetic properties of LaNi<sub>5</sub> and their effect on hydrogen desorption under the action of a magnetostatic field. *Heliyon* **2023**, *9*, 20311. [[CrossRef](#)] [[PubMed](#)]
26. Briki, C.; Belkhiria, S.; Almoneef, M.; Mbarek, M.; Jemni, A. Experimental study of the microstructures and hydrogen storage properties of the LaNi<sub>4</sub>Mn<sub>0.5</sub>Co<sub>0.5</sub> alloys. *Heliyon* **2023**, *9*, 17430. [[CrossRef](#)] [[PubMed](#)]
27. Belkhiria, S.; Briki, C.; Dhaou, M.H.; Jemni, A. Experimental study of a metal–hydrogen reactor’s behavior under the action of an external magnetostatic field during absorption and desorption. *Int. J. Hydrogen Energy* **2020**, *45*, 4673–4684. [[CrossRef](#)]
28. Yehui, C.; Xiangguo, Z.; Junfeng, X.; Huaqin, K. The comprehensive review for development of heat exchanger configuration design in metal hydride bed. *Int. J. Hydrogen Energy* **2022**, *47*, 2461–2490.
29. Saurabh, T.; Pratibha, S. Integration of metal hydride reactor with thermocline based heat storage system. *J. Energy Storage* **2023**, *59*, 106506.
30. Puchanee, L.; Nick, S.B.; Zhen, L.; Robert, F.; Emilie, S.; Mohammad, S.I. A novel design for faster hydrogen storage: A combined semi-cylindrical and central return tube heat exchanger. *J. Energy Storage* **2023**, *71*, 108018.
31. Shahin, S.; Mary, H.M.C. Different reactor and heat exchanger configurations for metal hydride hydrogen storage systems—A review. *Int. J. Hydrogen Energy* **2016**, *41*, 9462–9470.
32. Busra, A.; Mustafa, I.; Selahattin, C. Experimental analysis of hydrogen storage performance of a LaNi<sub>5</sub>–H<sub>2</sub> reactor with phase change materials. *Int. J. Hydrogen Energy* **2023**, *48*, 6010–6022.
33. Yang, Y.; Jianfeng, L.; Jing, D.; Weilong, W.; Jinyue, Y. Numerical simulation on the storage performance of a phase change materials based metal hydride hydrogen storage tank. *Appl. Energy* **2020**, *278*, 115682.
34. Nuaman, F.A.; Leqaa, A.M.; Abdulwahhab, H.M.; Shankar, S.; Bilal, J.M.A.; Mustafa, A.A. The effect of addition Ag and MnO<sub>2</sub> nanoparticles in the hydrogen storage of ethyl 2-((5-methoxybenzo[d]thiazol-2-yl)thio) acetate (organic: Inorganic nanohybrids). *J. Indian Chem. Soc.* **2022**, *99*, 100734.
35. Michael, U.N.; Sesha, S.S.; Ayala, R.P.; Ashok, K.; Yogi, G.; Elias, K.S. Nanomaterials for Hydrogen Storage Applications: A Review. *J. Nanomater.* **2008**, *2008*, 950967.
36. Andrii, L.; Julien, O.F.; Mohammad, F.; Jin-Yoo, S.; Young, S.L.; Jae-Hyeok, S.; Jihye, P.; Young, W.C. Enhancing the Hydrogen Storage Properties of AxBy Intermetallic Compounds by Partial Substitution: A Short Review. *Hydrogen* **2020**, *1*, 38–63.
37. Jain, R.K.; Ankur, J.; Shivani, A.; Lalla, N.P.; Ganesan, V.; Phase, D.M.; Jain, I.P. Characterization and hydrogenation of CeNi<sub>5-x</sub>Cr<sub>x</sub> (x = 0, 1, 2) alloys. *J. Alloys Compd.* **2007**, *430*, 165–169. [[CrossRef](#)]
38. Ryo, Y.; Takayuki, K.; Satoshi, K.; Daisuke, O.; Taku, J.S.; Chikashi, N.; An-Pang, T. Creating the hydrogen absorption capability of CeNi<sub>5</sub> through the addition of Al. *Int. J. Hydrogen Energy* **2017**, *42*, 21832–21840.
39. Ryota, T.; Ryo, Y.; Satoshi, K.; Chikashi, N.; An-Pang, T. Ability of hydrogen storage CeNi<sub>5-x</sub>Gax and Mg<sub>2</sub>Ni alloys to hydrogen ateacetylene. *Sci. Technol. Adv. Mater.* **2019**, *20*, 774–785.
40. Sumita, S.; Kuldeep, P. Investigations on Microstructures of Ball-milled MmNi<sub>5</sub> Hydrogen Storage Alloy. *Mater. Res. Bull.* **2016**, *73*, 284–289.
41. Masumeh, S.; Mohammad, J.; Seyed, M.A.; Seyed, M.G.M.S. Microstructure and thermodynamic assessment of MmNi<sub>5-x</sub>Al<sub>x</sub> hydrogen storage alloys. *Sādhanā* **2021**, *46*, 127.
42. Billur, S.; Farida, L.-D.; Michael, H. Metal hydride materials for solid hydrogen storage: A review. *Int. J. Hydrogen Energy* **2007**, *32*, 1121–1140.
43. Todorova, S.; Rangelova, V.; Mihaylov, L.; Spassov, T. Effect of hydrogen induced decrepitation on the hydrogen sorption properties of MmNi<sub>5</sub>. *Int. J. Electrochem. Sci.* **2020**, *15*, 4900–4907. [[CrossRef](#)]
44. Sumita, S.; Kuldeep, P. Effect of transition metals on ball-milled MmNi<sub>5</sub> hydrogen storage alloy. *Mater. Renew. Sustain. Energy* **2015**, *4*, 19.
45. Anil Kumar, E.; Prakash Maiya, M.; Srinivasa Murthy, S.; Viswanathan, B. Structural, hydrogen storage and thermodynamic properties of some mischmetal–nickel alloys with partial substitutions for nickel. *J. Alloys Compd.* **2009**, *476*, 92–97. [[CrossRef](#)]
46. Toyoto, S.; Hiroyuki, S.; Reina, U.; Junya, I.; Yuki, N.; Kazuki, O.; Shigeyuki, T.; Shin-ichi, O. Hydrogen Absorption Reactions of Hydrogen Storage Alloy LaNi<sub>5</sub> under High Pressure. *Molecules* **2023**, *28*, 1256.
47. Mingyi, C.; Dongxu, O.; Jingwen, W.; Jiahao, L.; Jian, W. Environmental pressure effects on thermal runaway and fire behaviors of lithium-ion battery with different cathodes and state of charge. *Process Saf. Environ. Prot.* **2019**, *130*, 250–256.
48. Rupali, N.; Sumita, S.; Sterlin, L.H.; Sandra, L.A.; Ashish, T.; Meenu, S.; Ramesh, A.; Sanjiv, S.; Varsha, K.; Sesha, S.S. Recent developments in state-of-the-art hydrogen energy technologies—Review of hydrogen storage materials. *Sol. Compass* **2023**, *5*, 100033.
49. Evangelos, I.G.; Chongming, W.; Simon, S.; Oliver, C. Metal-Hydride-Based Hydrogen Storage as Potential Heat Source for the Cold Start of PEM FC in Hydrogen-Powered Coaches: A Comparative Study of Various Materials and Thermal Management Techniques. *Hydrogen* **2022**, *3*, 418–432.
50. Anil Kumar, E.; Prakash Maiya, M.; Srinivasa Murthy, S. Influence of aluminium content on the dynamic characteristics of mischmetal based hydrogen storage alloys. *J. Alloys Compd.* **2009**, *470*, 157–162. [[CrossRef](#)]

51. Molinas, B.; Pontarollo, A.; Scapin, M.; Peretti, H.; Melnichuk, M.; Corso, H.; Aurora, A.; Mirabile, D.G.; Montone, A. The optimization of  $\text{MmNi}_{5-x}\text{Al}_x$  hydrogen storage alloy for sea or lagoon navigation and transportation. *Int. J. Hydrogen Energy* **2016**, *24*, 14484–14490. [[CrossRef](#)]
52. Apostolov, A.; Stanev, N.; Tcholakov, P. Hydrogen desorption characteristics of  $\text{MmNi}_{5-x}\text{Fe}_x$  compounds. *J. Less Common Metals* **1985**, *110*, 127–129. [[CrossRef](#)]
53. Alok, K.; Nithin, N.R.; Muthukumar, P. Parametric studies on  $\text{MmNi}_{4.7}\text{Fe}_{0.3}$  based reactor with embedded cooling tubes for hydrogen storage and cooling application. *J. Energy Storage* **2021**, *35*, 102317.
54. Miao, M.L.; Chang, C.W.; Chun, C.Y. Development of high-performance hydrogen storage alloys for applications in nickel-metal hydride batteries at ultra-low temperature. *J. Power Sources* **2021**, *491*, 229585.
55. Vinod, K.; Pukazhselvan, D.; Singh, S.K. Hydrogen Storage Characteristics of  $\text{MmNi}_{5-x}\text{M}_x$  ( $\text{M} = \text{Cu}, \text{Mn}$  and  $\text{Al}$ ). *Adv. Sci. Lett.* **2012**, *18*, 164–169.
56. Dhanesh, C.; Wen-Ming, C.; Anjali, T. Metal Hydrides for NiMH Battery Applications. Solution thermodynamics of hydrogen in the mischmetal- $\text{Ni}_8$  system with aluminium, manganese and tin substitutions. *J. Alloys Compd.* **1992**, *185*, 259–271.
57. Xiaobo, M.; Xuedong, W.; Hui, D.; Yongning, L. The relationship between discharge capacity of  $\text{LaNi}_5$  type hydrogen storage alloys and formation enthalpy. *J. Alloys Compd.* **2010**, *490*, 548–551.
58. Kwo-hsiung, Y.; Jean, N. The Current Status of Hydrogen Storage Alloy Development for Electrochemical Applications. *Materials* **2013**, *6*, 4574–4608.
59. Leah, M.; James, J.H.; Michel, L.T.; Peter, G.; Jan, P.E.; Juergen, E.; Nikolas, K.; David, M.A. A manganese hydride molecular sieve for practical hydrogen storage under ambient conditions. *Energy Environ. Sci.* **2019**, *12*, 1580–1591.
60. Snigdha, S.; Amrith, K.P.; Tripathi, M.M. Storage technologies for electric vehicles. *J. Traffic Transp. Eng. (Engl. Ed.)* **2020**, *7*, 340–361.
61. Shammya, A.; Sumon, R.; Kairat, K.; Asset, K.; Marzhan, M.K.; Kenzhebatyr, Z.B.; Abul, K.A. Emerging and Recycling of Li-Ion Batteries to Aid in Energy Storage, A Review. *Recycling* **2023**, *8*, 48.
62. Poojan, M.; Kondo-Francois, A.-Z. Titanium-iron-manganese ( $\text{TiFe}_{0.85}\text{Mn}_{0.15}$ ) alloy for hydrogen storage: Reactivation upon oxidation. *Int. J. Hydrogen Energy* **2019**, *44*, 16757–16764.
63. Satya, P.P.; Amritendu, R.; Soobhankar, P. Role of Mn-substitution towards the enhanced hydrogen storage performance in FeTi. *Int. J. Hydrogen Energy* **2022**, *47*, 9357–9371.
64. Peng, L.; Changlin, Z.; Dongfang, H.; Xingsheng, Z.; Zhichen, L.; Dejuan, H. Effect of introducing manganese as additive on microstructure, hydrogen storage properties and rate limiting step of Ti–Cr alloy. *Int. J. Hydrogen Energy* **2022**, *47*, 459–469.
65. Ben Lamine, A.; Bouazra, Y. Application of statistical thermodynamics to the olfaction mechanism. *Chem. Senses* **1997**, *22*, 67–75. [[CrossRef](#)]
66. Sghaier, W.; Ben Torkia, Y.; Bouzid, M.; Ben Lamine, A. Thermodynamic analysis of cooling cycles based on statistical physics modeling of ethanol adsorption isotherms. *Analysethermodynamique des cycles de refroidissement basée sur la modélisation physique statistique des isothermes à adsorption d'éthanol.* *Int. J. Refrig.* **2022**, *141*, 119–131. [[CrossRef](#)]
67. Belkhiria, S.; Briki, C.; Almoneef, M.; Dhaou, M.H.; Mbarek, M.; Jemni, A. Experimental and numerical study of hydrogen absorption in the  $\text{MmNi}_{5-x}\text{M}_x$  compound. *Int. J. Hydrogen Energy* **2023**, *51*, 29–40. [[CrossRef](#)]
68. Cousins, A.; Zohra, F.T.; Gray, E.M.; Webb, C.J.; Kochanek, M.; Edwards, S.; Schoeman, L. Alloy selection for dual stage metal-hydride hydrogen compressor: Using a thermodynamic model to identify metal-hydride pairs. *Int. J. Hydrogen Energy* **2023**, *48*, 28453–28459. [[CrossRef](#)]
69. Magda, P.; Julita, D.-W.; Tomasz, P.; Marek, P. The Influence of Cerium on the Hydrogen Storage Properties of  $\text{La}_{1-x}\text{Ce}_x\text{Ni}_5$  Alloys. *Energies* **2020**, *13*, 1437.
70. Alok, K.; Muthukumar, P.; Pratibha, S.; Anil Kumar, E. Absorption based solid state hydrogen storage system: A review. *Sustain. Energy Technol. Assess.* **2022**, *5*, 102204.
71. Bouaziz, N.; Briki, C.; Dhahri, E.; Jemni, A.; Ben Lamine, A. Experimental and theoretical investigation of absorption and desorption of hydrogen in the  $\text{LaNi}_4\text{Co}_{0.5}\text{Mn}_{0.5}$  alloy. *Chem. Eng. Sci.* **2022**, *251*, 117453. [[CrossRef](#)]
72. Bouaziz, N.; Ben Manaa, M.; Ben Lamine, A. Physicochemical and thermodynamic investigation of hydrogen absorption and desorption in  $\text{LaNi}_{3.8}\text{Al}_{1.0}\text{Mn}_{0.2}$  using the statistical physics modeling. *Results Phys.* **2018**, *9*, 1323–1334. [[CrossRef](#)]
73. Bajahzar, A.; Bouzid, M.; Briki, C.; Nasri, F.; Belmabrouk, H.; Jemni, A. Experimental and numerical study of the isotherms and determination of physicochemical parameters of the hydrogen absorption/desorption process by the metal hydrides. *Int. J. Hydrogen Energy* **2020**, *45*, 15281–15293. [[CrossRef](#)]

**Disclaimer/Publisher's Note:** The statements, opinions and data contained in all publications are solely those of the individual author(s) and contributor(s) and not of MDPI and/or the editor(s). MDPI and/or the editor(s) disclaim responsibility for any injury to people or property resulting from any ideas, methods, instructions or products referred to in the content.